

Article

# Poly(vinyl benzoate)-b-poly(diallyldimethyl ammonium TFSI)-b-poly(vinyl benzoate) Triblock Copolymer Electrolytes for Sodium Batteries

Pierre L. Stigliano <sup>1,2</sup> , Antonela Gallastegui <sup>2</sup>, Carlos Villacis-Segovia <sup>2</sup>, Marco Amores <sup>1</sup> , Ajit Kumar <sup>1</sup>, Luke A. O'Dell <sup>1</sup>, Jian Fang <sup>3</sup>, David Mecerreyes <sup>2,4</sup> , Cristina Pozo-Gonzalo <sup>1,5,6</sup>  and Maria Forsyth <sup>1,4,\*</sup> 

- <sup>1</sup> Institute for Frontier Materials, Deakin University, Geelong, VIC 3216, Australia; pstigliano@deakin.edu.au (P.L.S.); marco.amores@deakin.edu.au (M.A.); ajit.kumar@deakin.edu.au (A.K.); luke.odell@deakin.edu.au (L.A.O.); cristina.pozo@deakin.edu.au (C.P.-G.)
- <sup>2</sup> POLYMAT, University of the Basque Country UPV/EHU, 20018 Donostia-San Sebastian, Spain; antonela.gallastegui@polymat.eu (A.G.); carlos.villacis@polymat.eu (C.V.-S.); david.mecerreyes@ehu.es (D.M.)
- <sup>3</sup> College of Textile and Clothing Engineering, Soochow University, Suzhou 215123, China; jian.fang@suda.edu.cn
- <sup>4</sup> Ikerbasque, Basque Foundation for Science, María Díaz de Haro 3, 48013 Bilbao, Spain
- <sup>5</sup> ARAID Foundation, Av. de Ranillas 1-D, 50018 Zaragoza, Spain
- <sup>6</sup> Instituto de Carboquímica (ICB-CSIC), Miguel Luesma Castán, 4, 50018 Zaragoza, Spain
- \* Correspondence: maria.forsyth@deakin.edu.au

**Abstract:** Block copolymers (BCPs) as solid electrolytes for batteries are usually designed to have an ion-solvating block for ion conduction and an ionophobic block for providing mechanical strength. Here, we show a novel solid polymer electrolyte (SPE) for sodium batteries based on a poly(vinyl benzoate)-b-poly(diallyldimethyl ammonium bis(trifluoromethanesulfonyl)imide) PVB<sub>x</sub>-b-PDADMATFSI<sub>y</sub>-b-PVB<sub>x</sub> ABA triblock copolymer. The SPE triblock copolymer comprises a polymerized ionic liquid (PIL) ion-solvating block combined with NaFSI salt as an internal block and an ionophilic PVB as an external block. Four distinct compositions with varying chain lengths of the blocks were synthesized by reversible addition–fragmentation chain-transfer (RAFT) polymerization. The neat copolymers were subsequently mixed with NaFSI in a 2:1 mol ratio of Na to ionic monomer units. Through comprehensive analysis using differential scanning calorimetry (DSC), Fourier-transform infrared spectroscopy (FTIR), and nuclear magnetic resonance (NMR), it was revealed that the ion coordination within the polymer–salt mixtures undergoes changes based on the composition of the starting neat polymer. Electrochemical evaluations identified the optimal composition for practical application as PVB<sub>11.5K</sub>-b-PDADMATFSI<sub>33K</sub>-b-PVB<sub>11.5K</sub>, showing an ionic conductivity at 70 °C of  $4.2 \times 10^{-5} \text{ S cm}^{-1}$ . This polymer electrolyte formulation was investigated for sodium in Na|Na symmetrical cells, showing an overpotential of 200 mV at 70 °C at 0.1 mA cm<sup>-2</sup>. When applied in a sodium–air battery, the polymer electrolyte membrane achieved a discharge capacity of 1.59 mAh cm<sup>-2</sup> at 50 °C.

**Keywords:** polymer electrolytes; block copolymers; sodium batteries; sodium-air batteries



**Citation:** Stigliano, P.L.; Gallastegui, A.; Villacis-Segovia, C.; Amores, M.; Kumar, A.; O'Dell, L.A.; Fang, J.; Mecerreyes, D.; Pozo-Gonzalo, C.; Forsyth, M. Poly(vinyl benzoate)-b-poly(diallyldimethyl ammonium TFSI)-b-poly(vinyl benzoate) Triblock Copolymer Electrolytes for Sodium Batteries. *Batteries* **2024**, *10*, 125. <https://doi.org/10.3390/batteries10040125>

Academic Editors: Atsushi Nagai and Catia Arbizzani

Received: 26 February 2024

Revised: 17 March 2024

Accepted: 5 April 2024

Published: 8 April 2024



**Copyright:** © 2024 by the authors. Licensee MDPI, Basel, Switzerland. This article is an open access article distributed under the terms and conditions of the Creative Commons Attribution (CC BY) license (<https://creativecommons.org/licenses/by/4.0/>).

## 1. Introduction

The landscape of energy harvesting and storage is rapidly evolving, driven by the need to transition from fossil fuels to renewable energy sources. Among the various energy storage solutions, battery technology has been drawing much attention in research. On the one hand, a lot of effort is being put into achieving batteries that exhibit enhanced performance, particularly in terms of their overall capacity [1]. This necessity arises from the growing demand for energy storage solutions across various industries and applications [2]. On the other hand, the current political scenario demands that safety, cost, and sustainability

of battery life cycles be imperative characteristics when investigating new battery concepts and designs [3–6]. The potential problems related to battery use and disposal are becoming more and more obvious as batteries are integrated into every aspect of our daily lives.

Due to the great source of raw materials, sodium-based batteries are emerging as a competitive technology in the field of energy storage to supplement the rising need for higher energy densities and storage capacities, currently sustained primarily by the well-established lithium ion technology [7–10]. Current sodium-based batteries share with lithium ion technology the safety concerns linked to flammable and toxic liquid electrolytes. Because of their simplicity of processing and low flammability, polymer electrolytes have found a growing research interest [11–16]. Furthermore, polymers have a number of structural choices that span from linear homopolymers to more complex architectures like block copolymers, which allow for tailoring of properties and application to a variety of applications [15–23].

Among the diverse options within polymer electrolytes, block copolymer electrolytes (BCEs) have emerged as particularly promising. BCEs exhibit phase-separated nanostructured morphologies, offering independent tuning of thermal, mechanical, and electrochemical properties—a key advantage for adapting to varied applications [24–28]. This innovative approach involves the synthesis of polymer electrolytes containing a ‘soft’ block that coordinates with metal ions (i.e., Li and Na) for ionic transport and a ‘rigid’ block for mechanical strength and structural support [18,19,29]. The need for precisely tailored blocks requires synthetic methods that can achieve the targeted molecular weights and distributions with accuracy. Some polymerization techniques defined as living or controlled, including anionic, cationic, ring-opening metathesis polymerization (ROMP), atom transfer radical polymerization (ATRP), and RAFT, enable the achievement of consistent and measurable structure–property relationships [25]. Among these techniques, RAFT has gained popularity for its versatility in monomer and condition selection, accommodating various initiation methods [30–33]. For the mechanical block, a “rigid” polymer with a high glass transition, such as polystyrene and polymethylmethacrylate, is typically chosen [29,34–36]. The immiscibility of individual blocks results in phase-separated nanostructured morphologies, enhancing the mechanical properties of these copolymers.

Various polymer chemistries have been explored for ion solvation, with polyethylene oxides, polycarbonates, and poly(ionic liquid)s among the most investigated [8,17,37]. In particular, the poly(ionic liquid) backbone poly(diallyldimethyl ammonium bis trifluoromethanesulfonimide), known as PDADMATFSI, has been demonstrated to have great versatility for lithium and sodium batteries [38,39]. Interestingly, previous studies have shown the potential of block copolymers with PDADMA-based ion solvation blocks [11,29,38,40–42]. Thus, Malunavar et al. [29] reported a free-standing polymer electrolyte membrane composed of a polystyrene (PS) block and PS-*b*-PDADMATFSI-*b*-PS block copolymer and NaFSI salt mixture, which demonstrated an ionic conductivity of  $10^{-3} \text{ S cm}^{-1}$  and sodium transference number of 0.34 at 70 °C using a mol ratio of DADMATFSI:NaFSI of 1:2. The polymer electrolyte also achieved a stable overpotential of 300 mV when cycled in Na-symmetric systems up to  $0.2 \text{ mA cm}^{-2}$  and a specific capacity of  $118 \text{ mAh g}^{-1}$  at a C/20 rate at 70 °C in a Na|NaFePO<sub>4</sub> cell. However, in that investigation, it was suggested that the mechanical stability of the polymer electrolyte membrane is compromised by the low molecular weight of the polystyrene mechanical block ( $2000 \text{ g mol}^{-1}$ ) and the lack of control and high dispersity observed in the RAFT copolymerization process. With such low molecular weights and high dispersity values, the mechanical properties would be limited by the inability of the short polystyrene chains to achieve molecular entanglement.

To overcome the mechanical issues encountered by Malunavar et al., high-molecular-weight mechanical blocks need to be investigated. For example, Makhlooghiyazd et al. [43] reported a solid polymer electrolyte membrane composed of another poly(ionic liquid) block copolymer NaFSI salt and polystyrene-block-poly(acrylethyl(butylimidazolium bis (trifluoromethanesulfonyl)imide)) (PS-PEA(BuImTFSI)) AB block copolymer, with a polystyrene

mechanical block having a molecular weight of 24,000 g mol<sup>-1</sup>. When the molar ratio between NaFSI and polymer was 1:2.5, the SPE attained an ionic conductivity of  $4.2 \times 10^{-5}$  S cm<sup>-1</sup> at 70 °C. The ionic conductivity obtained in Makhlooghiadz's work was, however, significantly lower than that of Malunavar et al. ( $10^{-5}$  vs.  $10^{-3}$  S cm<sup>-1</sup> at 70 °C, respectively). The difference in ionic conductivity observed can be related to the lower volume fraction of the conductive domain. This hypothesis was investigated by Young and Epps [44], who reported a decrease in ionic conductivity in PS-*b*-PEO/Li salt polymer electrolytes as the volume fraction of PEO (conducting block) decreased. To overcome the issues related to the difficult ion conduction stemming from the presence of a non-conductive mechanical block, Cao et al. [45] investigated block copolymer electrolytes with double conductive nanophases. The LiTFSI-doped poly(propylene monothiocarbonate)-*b*-poly(ethylene oxide) (PPMTC-*b*-PEO) block copolymers achieved high ionic conductivity at room temperature ( $10^{-4}$  S cm<sup>-1</sup>) and storage moduli 1–4 orders of magnitude higher than LiTFSI/PEO electrolytes.

In this article, we explore an ABA triblock copolymer electrolyte (BCE) designed for sodium battery applications, consisting of poly(vinyl benzoate)-*b*-poly(diallyldimethylammonium bis(trifluoromethanesulfonyl)imide)-*b*-poly(vinyl benzoate) (PVB-*b*-PDADMATFSI-*b*-PVB). The choice of poly(vinyl benzoate) for the mechanical block stems from two key factors. The presence of a benzoate ring in the backbone confers rigidity and mechanical strength to the polymer system. In addition, we anticipate the possibility of coordination of Na ions with the oxygen in the vinyl benzoate block. To study the influence of PVB as a “conductive” mechanical block on the physiochemical and electrochemical properties of polymer electrolytes, we synthesized four different samples with different chain lengths of PVB and PDADMATFSI, and NaFSI was added for evaluation of the polymer compositions in solid polymer electrolytes. The choice of mixed anions (FSI/TFSI) in the system is motivated by previous research showing the superior physiochemical and electrochemical properties of mixed anions systems in ionic liquid-based and polymer electrolytes [29,43,46–48]. The various compositions of neat block copolymers with different chain lengths of PVB and PDADMATFSI were mixed with NaFSI in a fixed NaFSI:DADMATFSI ratio, and the physiochemical properties of the electrolyte membranes were explored via DSC, solid-state NMR, FTIR, and EIS. The most promising formulation was then further studied to evaluate the potential applicability of this solid polymer electrolyte in symmetrical sodium metal cells and a sodium–air battery as a probe of concept.

## 2. Results and Discussion

### 2.1. Synthesis and Characterization of Poly(vinyl benzoate)-*b*-poly(diallyldimethyl ammonium TFSI) PVB-*b*-PDADMATFSI-*b*-PVB Triblock Copolymers

For the synthesis of the PVB-*b*-PDADMATFSI-*b*-PVB triblock copolymers, we used a similar strategy to the one previously reported for the synthesis of triblock copolymers based on polystyrene [29] (Figure 1a). The triblock copolymers were synthesized by RAFT polymerization employing a macrochain transfer agent (MacroCTA) initiator based on a water-soluble xanthogenate-based chain transfer agent (CTA) with a short polyacrylamide unit. This difunctional CTA was used to initiate the controlled radical polymerization of the diallyldimethylammonium chloride (DADMACl) monomer as reported before (see the methods in the Supplementary Materials) [39]. Once the poly(diallyldiammonium chloride) PDADMACl polymer was obtained, an anion exchange reaction was carried out with LiTFSI to yield poly(diallyldiammonium bis(trifluoromethanesulfonyl)imide) (PDADMATFSI). Two chain lengths of PDADMATFSI were investigated in this work: 33 K (named as long) and 17.5 K (named as short), as shown in Table 1. The obtained gas permeation chromatography (GPC) traces of PDADMACl<sup>-</sup> shown in Figure 1b showed that the molecular weight corresponded to the expected values and the dispersity of the PDADMACl<sup>-</sup> was low. In the final step, the difunctional PDADMATFSI was used as macro-CTA for the polymerization of vinyl benzoate, as shown in Figure 1. After polymerization, the final PVB-*b*-PDADMATFSI-*b*-PVB triblock copolymers were isolated in high yields.

Table 1 shows the synthesized triblock copolymer with the nomenclature assigned to each sample. The triblocks were named BCP-XXYY, where XX is the molecular weight of PVB and YY is the molecular weight of PDADMATFSI, expressed in  $\text{Kg mol}^{-1}$  and rounded to the highest integer. The composition of the triblock copolymers was calculated by  $^1\text{H-NMR}$  by integrating the signals associated with each block, as shown in Figures S4–S7. FTIR analyses (Figure 1c) confirmed the chemical structure, and signals associated with each block were identified. The FTIR absorption bands for each block [PDADMA][TFSI] and PVB are shown in the figure and summarized in Table S1. Regarding [PDADMA][TFSI], the bands assigned to the polymeric cation  $[\text{P}(\text{DADMA})]^+$  are 1670 ( $\beta\text{C-N}$ ) and 1476 ( $\delta\text{CH}_3$ )  $\text{cm}^{-1}$  [49], while the bands related to the anion  $[\text{TFSI}]^-$  are observed at 1349 and 1332 ( $\nu_{\text{as}}\text{SO}_2$ ), 1175 ( $\nu_{\text{as}}\text{CF}_3$ ), 1132 ( $\nu_{\text{s}}\text{SO}_2$ ), 1053 ( $\delta\text{CF}_3$ ), 789 ( $\text{S-N stretch}/\delta\text{CF}_3$ ), 741 ( $\nu_{\text{s}}(\text{S-N-S})$ ), and 656 ( $\delta(\text{SNS})$ )  $\text{cm}^{-1}$ , as reported also in the literature [50]. The bands assigned to PVB are 1711 ( $\text{C=O}$ ), 1584 ( $\text{C=C}$  of the benzoate ring), 1451 ( $\text{C-C}$  of the benzoate ring), 1269 ( $\text{C-O}$ ), and 707 ( $\text{C-H}_{\text{oop}}$ )  $\text{cm}^{-1}$  [51,52].

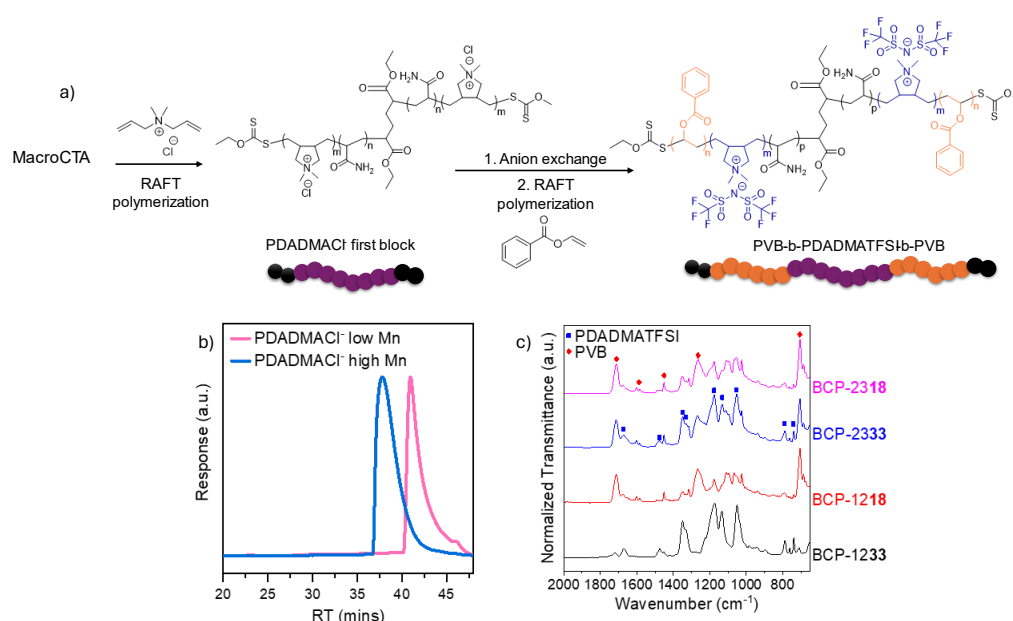


**Figure 1.** (a) Synthesis scheme of PVB-b-PDADMATFSI-PVB block copolymers through RAFT polymerization. GPC chromatograms versus elution time are shown for PDADMACl and final triblock copolymers; (b) GPC traces of the two chain lengths of PDADMACl<sup>−</sup>; (c) FTIR spectra of the four compositions of neat BCPs.

**Table 1.** Conversion, theoretical, and experimental molecular weight for all steps of PVB-b-PDADMATFSI-b-PVB synthesis.

Sample	Conversion <sup>a</sup> (%)	$M_{n,th}$ ( $\text{kg mol}^{-1}$ )	$M_{n,exp}$ ( $\text{kg mol}^{-1}$ )	PI ( $M_n/M_w$ )	Name
X-PAm-DiEst-PAm-X	66	2.8	1.9 <sup>b</sup>	-	-
PDADMACl-high Mn	50	21.5	17.7 <sup>c</sup>	1.7	-
PDADMACl-low Mn	50	11.4	5.4 <sup>c</sup>	1.9	-
PDADMATFSI-high Mn	90	36.8	33.1	-	-
PDADMATFSI-low Mn	95	18.4	17.5	-	-
PVB <sub>11.5K</sub> -b-PDADMATFSI <sub>33K</sub> -b-PVB <sub>11.5K</sub>	80	13	10.4 <sup>a</sup>	2.1	BCP-1233
PVB <sub>11.5K</sub> -b-PDADMATFSI <sub>17.5K</sub> -b-PVB <sub>11.5K</sub>	99	13	12.8 <sup>a</sup>	2.5	BCP-1218
PVB <sub>22.5K</sub> -b-PDADMATFSI <sub>33K</sub> -b-PVB <sub>22.5K</sub>	87	26	20.8 <sup>a</sup>	2.2	BCP-2333
PVB <sub>22.5K</sub> -b-PDADMATFSI <sub>17.5K</sub> -b-PVB <sub>22.5K</sub>	94	26	24.4 <sup>a</sup>	2.2	BCP-2318

<sup>a</sup> Determined by  $^1\text{H NMR}$ . <sup>b</sup> Determined by MALDI-TOF. <sup>c</sup> Determined by SEC.

Thermal characterization of all BCPs was carried out by DSC and TGA. DSC results can be observed in Figure 2a, where a single glass transition temperature ( $T_g$ ) was observed within the temperature range of 60 to 70 °C for all triblocks, which is attributed to the poly(vinyl benzoate) (PVB) block, while the  $T_g$  of PDADMATFSI could not be observed. It has already been shown in the literature that it is difficult to observe the  $T_g$  of PDADMA-based ionomers. Yunis et al. employed DMA to be able to observe the  $T_g$  of PDADMATFSI at 116 °C [53]. Notably, compositions characterized by longer PVB chains, namely BCP-2333 and BCP-2318, exhibited elevated glass transition temperatures, consistently hovering around 69 °C. In contrast, compositions BCP-1233 and BCP-1218, featuring shorter PVB chains, displayed comparatively lower  $T_g$  values of 60 °C and 62 °C, respectively. TGA results can be seen in Figure 2b, where a degradation higher than 5 wt% can be observed at temperatures higher than 263 °C for all BCPs, demonstrating the excellent thermal stability of these polymers. A clear contribution of PVB and PDADMATFSI is shown in the thermogravimetric analysis, where PVB degrades at lower temperatures than the PDADMATFSI block ones. The decomposition of PVB starts at 263 °C for all samples and reaches a plateau at weight loss % correlated to the PVB chain length and mol ratio: samples with short chains of PVB and a lower PVB mol ratio undergo a smaller weight loss (BCP-1233 > BCP-1218 > BCP-2333 > BCP-2318). The second sharp weight loss occurs in the range of 365–380 °C, with all samples reaching a remaining weight of 5–7 wt%.

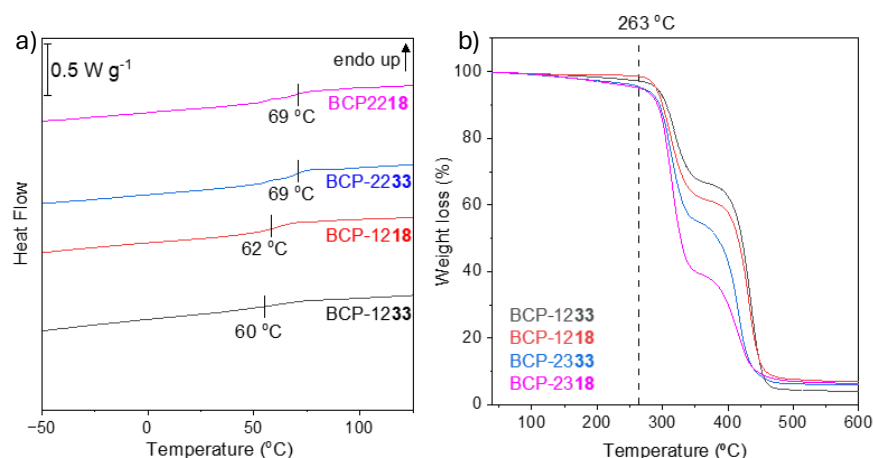


**Figure 2.** (a) DSC traces of the four compositions of neat BCP from  $-50$  °C to  $150$  °C, second heating at  $40$  K/min; (b) TGA traces of the four compositions of neat BCP up to  $600$  °C,  $10$  K/min.

Finally, TEM analyses (Figure S8) were performed on two copolymers with different compositions: long PDADMATFSI/short PVB (BCP-1233) vs. short PDADMATFSI/long PVB (BCP-2318). In both compositions, two main structures are visible: light gray aggregates and elongated wormlike fibril-like structures. These materials were difficult to section, and thus the expected phase separation of block copolymers was not obvious from the TEM analysis.

#### Solid Polymer Electrolytes Based on Blends of NaFSI and PVB-b-PDADMATFSI-b-PVB Triblock Copolymers

Solid polymer electrolytes were prepared by solvent-casting solutions of the block copolymers and the salt NaFSI, as represented in Figure 3a, resulting in flexible solid membranes. Four triblock copolymers with different lengths and compositions were mixed with NaFSI (in a mol ratio of 2:1 with respect to the DADMATFSI unit vs. NaFSI). The 2:1 molar ratio between NaFSI and DADMATFSI monomer units was chosen based on previous studies [29], which showed that this specific ratio yielded improved transport properties, characterized by notable Na<sup>+</sup> ion dynamics, as observed through NMR analyses, coupled with high ionic conductivity. The samples were named BCP-XXYY-Na, where BCP-XXYY refers to the neat polymer used.

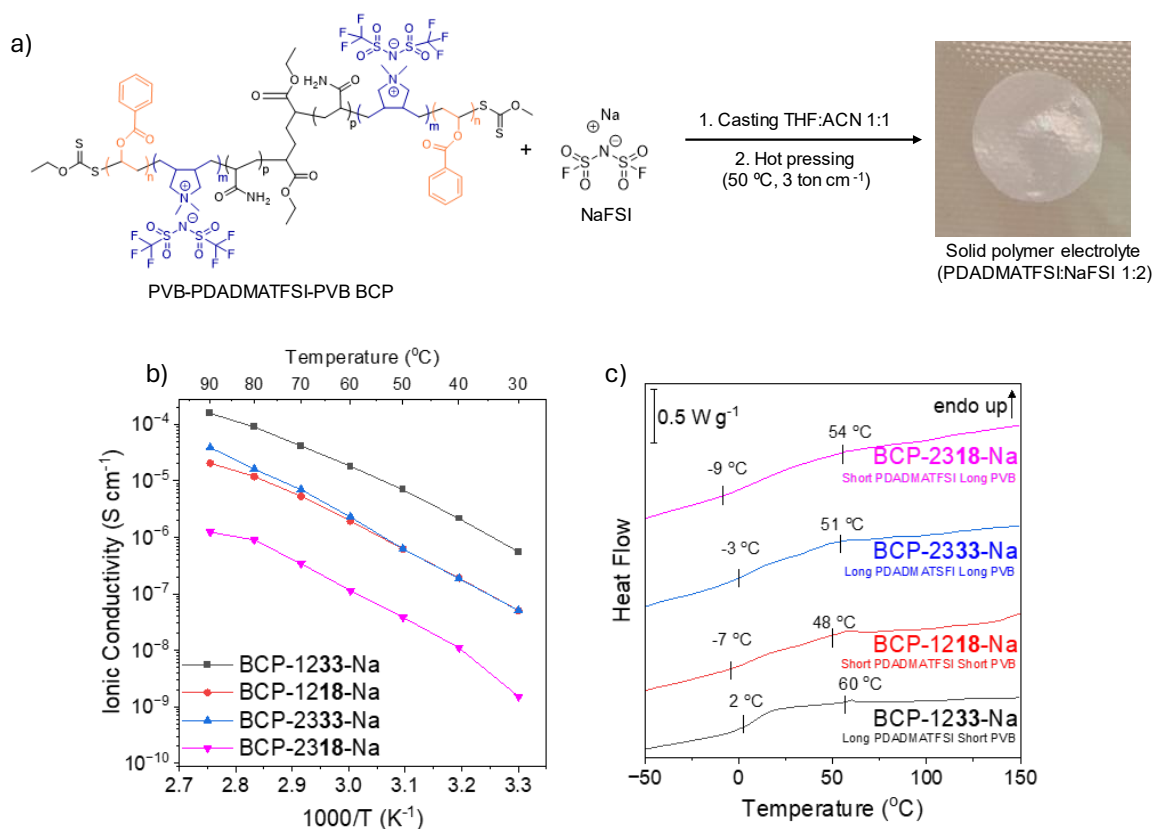


**Figure 3.** (a) Casting method for NaFSI/PVB-b-PDADMATFSI-b-PVB BCP polymer electrolyte membranes. (b) Temperature-dependent ionic conductivity of membrane with a 2:1 Na:PDADMATFSI mol ratio for all four compositions of neat polymer between 30 and 90 °C. (c) DSC traces of membrane with a 2:1 Na:PDADMATFSI mol ratio for all four compositions of neat polymer from −50 °C to 150 °C, second heating at 40 K/min.

Figure 3b shows the ionic conductivity of the four BCP compositions with a 2:1 Na:PDADMA mol ratio in the range of temperature between 30 °C and 90 °C. At 50 °C, the trend in ionic conductivity is observed as follows: BCP-1233-Na exhibits the highest value at  $6.9 \times 10^{-6} \text{ S cm}^{-1}$ , followed by BCP-2333-Na and BCP-1218-Na with identical values of  $6.2 \times 10^{-7} \text{ S cm}^{-1}$ , and BCP-2318-Na displaying the lowest conductivity at  $3.8 \times 10^{-8} \text{ S cm}^{-1}$ . Compared to previous works with PDADMATFSI, the ionic conductivity observed in this work is lower by an order of magnitude [11,29]. Notably, low values of glass transition temperature are deemed crucial for achieving polymer materials with elevated ionic conductivity. Interestingly, BCP-1233-Na showed the highest T<sub>g</sub> values for both the PDADMATFSI block (2 °C) and PVB (60 °C) (Figure 3c). These results suggest the occurrence of a decoupled behavior, as previously reported by Malunavar et al. [29], where the ion conductivity occurs via ion hopping or structural rearrangement ion diffusion. Additionally, the observed trend in ionic conductivity aligns with observations made from the investigation of the Na environment through NMR spectroscopy, as they will be discussed further later.

The temperature-dependent ionic conductivity curve obtained for the samples could be fitted using Equation (1):

$$\sigma = \sigma_0 \left( \frac{-E_a}{kT} \right) \quad (1)$$

where  $\sigma_0$  is the pre-exponential factor,  $E_a$  represents the activation energy,  $k$  denotes the Boltzmann constant, and  $T$  is the absolute temperature. The calculated values for the activation energy of the sample were in the range of 85–90 kJ/mole. The activation energy obtained from the Arrhenius plot of ionic conductivity can be related to the energy barrier

for the ions in the system to diffuse. Compared to other systems, the activation energy calculated for these samples is larger (values are in general found to be <50 kJ/mol), suggesting the diffusion of Na<sup>+</sup> ions in our systems is more difficult [54–56]. The high activation energy and hindered diffusion of ions in the systems investigated could affect the electrochemical performance, with an increased overpotential for Na plating/stripping, reducing the limiting current for cycling, for example.

From the DSC analysis shown in Figure 3c, we appreciate the presence of two  $T_g$  values in each sample, one related to PDADMATFSI and one related to PVB. This confirms the phase separation expected in block copolymer electrolytes, with each block maintaining distinct properties, as observed from TEM analysis of the polymer electrolyte membranes (Figure S9). The temperature range in which the glass transitions occur appears to be broad; thus,  $T_g$  values were obtained from the onset of the first derivative of the thermograph.

As mentioned earlier for the neat BCP measurements, the  $T_g$  of PDADMATFSI was found in the literature to be 116 °C. As expected, the addition of NaFSI significantly lowers the  $T_g$  of PDADMATFSI, as it has been previously reported the plasticizing effect of the Na salt in PDADMATFSI polymers, where a decrease in the TFSI-DADMA interactions resulted in a large decrease in  $T_g$  to values around 0 °C [11,29]. For all four membranes, a distinct glass transition temperature related to the PDADMATFSI block is consistently observed between –9 and 2 °C. The influence of PDADMATFSI chain length on  $T_g$  becomes evident, with longer chains correlating to higher temperatures: BCP-1233-Na > BCP-2333-Na > BCP-1218-Na > BCP-2318-Na. Moreover, the trend in  $T_g$  of PDADMATFSI seems linked to the PDADMATFSI:PVB mol ratio, suggesting that higher mol ratios result in higher  $T_g$  values. Regarding PVB, its  $T_g$  in the electrolyte membranes generally occurs at lower temperatures compared to neat polymers, except for BCP-1233-Na, where the  $T_g$  of the PVB chain aligns with that of the neat polymer BCP-1233. The  $T_g$  of PVB follows a specific order: BCP-1233-Na > BCP-2318-Na > BCP-2333-Na > BCP-1218-Na. Notably, the addition of NaFSI has a pronounced effect on PVB  $T_g$ , especially when the chains are longer (BCP-2333-Na and BCP-2318-Na), with the most significant variation observed in BCP-2333-Na, where the  $T_g$  decreases from 69 °C to 51 °C. From this investigation, we can see how two different behaviors are observed by varying the chain length of the two blocks and, explicitly, how longer PVB chains result in partial coordination with Na ions. As will be discussed later, this behavior was also found during the investigations of the interactions between Na salt and polymer via FTIR analysis, where the PVB chain is found to interact to some extent with Na<sup>+</sup> in these block copolymers.

NMR spectroscopy serves as a comprehensive tool to investigate both the chemical environment surrounding ionic species and their dynamics in these block copolymer electrolytes. The focus of these methods was to probe the structure and ion transport as they were influenced by the chain lengths of the polymer blocks. Figure 4a presents the solid-state magic angle spinning (MAS) NMR spectra for <sup>23</sup>Na, revealing two major peaks across all samples.

The <sup>23</sup>Na NMR analysis reveals intriguing coordination environments and ion dynamics. Two prominent peaks consistently appear across all samples. The peak at 7.3 ppm (peak 1) is attributed to sodium coordination with the oxygen in polyvinyl benzoate (PVB), due to its proximity to the chemical shift observed in sodium carbonate. Remarkably, the chemical shift at 7.3 ppm remains invariant throughout the diverse samples, indicating a stable coordination environment. The width of the peak also remains relatively narrow, indicating that the Na<sup>+</sup> environment is symmetric.

The width at half-maximum (FWHM) for <sup>23</sup>Na can also be used as an indicator of the mobility of Na ions and fast ion exchange in the system [57]. The investigation into the FWHM frequencies of the resonance at around –20 ppm reveals an interesting trend (black line in Figure 4b); the peak narrows from BCP-1233-Na to BCP-2333-Na, reaching a minimum, and then perceptibly widens in BCP-2318-Na. This suggests that the mobility of these ions is compromised in BCP-2318-Na, as reflected by a significantly larger FWHM.

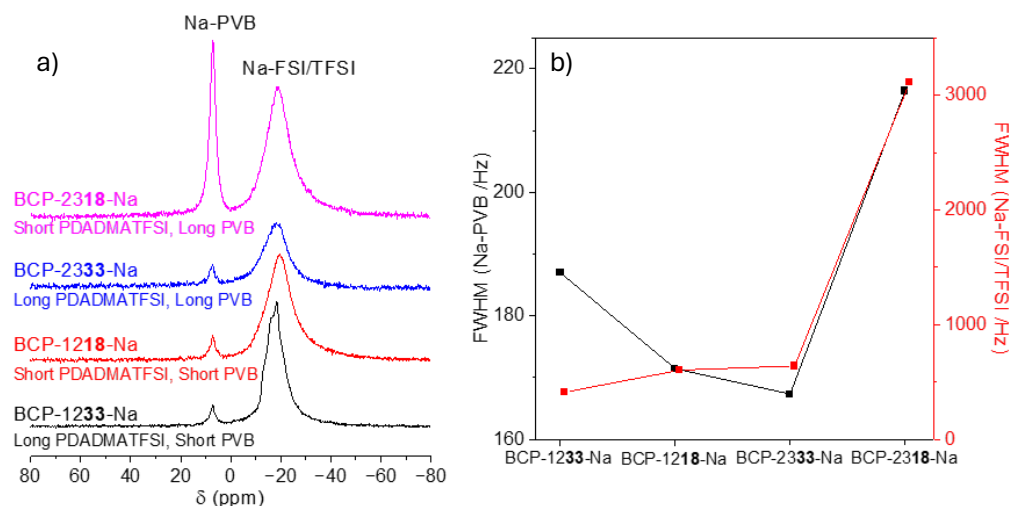


**Figure 4.** (a)  $^{23}\text{Na}$  MAS-NMR spectra of the membranes with a 2:1 Na:DADMATFSI mol ratio for all four compositions of neat polymer at 50 °C; (b) full width half-maximum (fwhm) frequencies of  $^{23}\text{Na}$  as a function composition (black represents the Na-PVB resonance and red Na-FSI/TFSI).

This second peak is associated with  $\text{Na}^+$  ions that are coordinated by the anions (FSI/TFSI). This peak shows a characteristic second-order quadrupolar line shape for sample BCP-1233(2) (short PVB, long PDADMATFSI), indicating a well-defined  $\text{Na}^+$  solvation environment. These quadrupolar features are broadened in the other samples, which may result from an increased variation in  $\text{Na}^+$  solvation environments and/or changes in the dynamics of the sodium ion in these systems. The trend in FWHM, depicted by the red line in Figure 4b, shows that BCP-2318-Na exhibits a significantly wider peak (3111 Hz) compared to BCP-1233-Na, BCP-1218-Na, and BCP-2333-Na, indicating diminished sodium ion mobility in BCP-2318-Na consistent with the lowest ionic conductivity. The peak positions of the Na-FSI/TFSI peaks fall between  $-18$  and  $-20$  ppm for all samples. This position, which will result from a combination of chemical shift and second-order quadrupolar shift, is situated at less negative values compared to other systems utilizing NaFSI and PDADMATFSI [29]. It was observed in previous works that the TFSI anion generally interacts more strongly with Na than the FSI anion [57]. The difference in chemical shift observed in the systems under investigation here suggests stronger coordination of sodium with the FSI anion in this case. Moreover, among the different systems in this study, it appears that the chain length of the PDADMATFSI block influences the coordination of the sodium ion. In the samples with longer PDADMATFSI chains (BCP-1233-Na and BCP-2333-Na), the peak appears at  $-18$  ppm, while in the samples with shorter PDADMATFSI chains (BCP-1218-Na and BCP-2318-Na), the peak is situated at slightly lower chemical shifts. This result aligns with the hypothesis that the Na ion coordination environment is shared between PDADMATFSI and PVB when the former has shorter chains and the latter longer chains, as anticipated in the explanation of the DSC thermograms and consistent with the FTIR analysis below.

The ratio between the integrals of the two peaks (Figure S10) provides a quantification of the two observed sodium coordination environments. This ratio remains constant in BCP-1233-Na, BCP-1218-Na, and BCP-2333-Na (0.05) but conspicuously increases in BCP-2318-Na (0.35), indicative of the larger share of Na ions coordinating with the PVB chain. Finally, it should be noted that the resolution of these separate peaks indicates that these two distinct populations of sodium ions do not undergo any appreciable exchange on the time scale of the NMR experiment (ms).

From these observations, we can see that the main coordination of sodium is with FSI and TFSI, making the PDADMATFSI the major ion conductor in the polymer electrolyte samples, as expected.

Infrared spectroscopy (Figure 5 and Figure S11) has been employed to investigate the possible interactions/complexation between the different constituents in the block copolymer electrolyte. The spectroscopic analysis investigated the variation in interactions occurring when the same mol ratio of Na:PDADMA (2:1) was added to the different formulations of the neat block copolymers. Specifically, the study focused on how the chain length of the two main components (PDADMATFSI and PVB) and their mol ratio (PDADMATFSI:PVB) influence the coordination of the Na cation when introduced as NaFSI. BCP-1233-Na and BCP-2318-Na materials have been the focus of this study based on their antithetical compositions of the starting polymer: BCP-1233 has long chains of PDADMATFSI and short chains of PVB; BCP-2318 has short chains of PDADMATFSI and long chains of PVB.

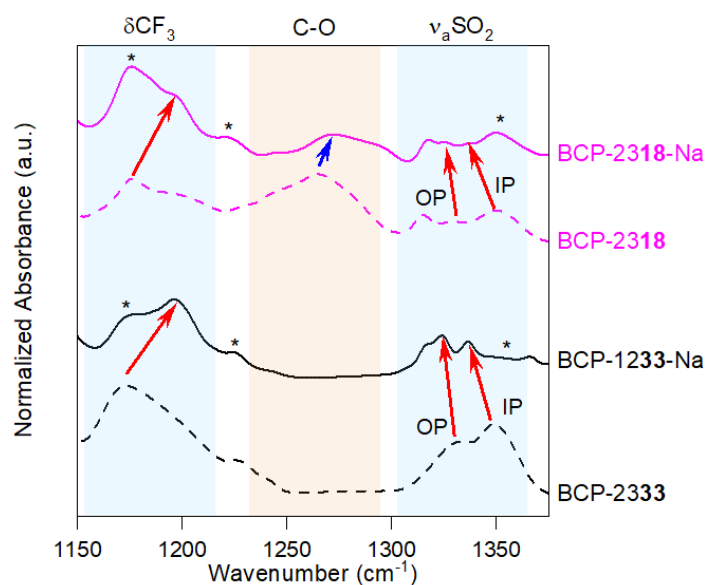


**Figure 5.** FTIR spectra of neat BCP and BCP-NaFSI mixtures with a 2:1 Na:DADMA mol ratio for BCP-1233(-Na) and BCP-2318(-Na). Star symbols denote bands arising from the NaFSI salt.

For the BCP-1233-Na (black solid line), the bands from the  $[\text{TFSI}]^-$  anion show a shift in the peak as expected, with the most discernible changes being associated with the  $\text{SO}_2$  moiety. The peaks observed in the neat polymer at  $1333\text{ cm}^{-1}$  and  $1349\text{ cm}^{-1}$  have been previously related to the stretching in-phase and out-of-phase of the two sulfonyl groups in the TFSI anion. The peak at  $1333\text{ cm}^{-1}$  has been assigned to the cis conformer, while the peak at  $1349\text{ cm}^{-1}$  is assigned to the trans conformer of the anion [58–60]. When NaFSI is added to the neat polymer in the SPE, these two peaks both show a peak shift: the  $\nu_{\text{aSO}_2}$  OP shifts from  $1333$  to  $1322\text{ cm}^{-1}$  and  $\nu_{\text{aSO}_2}$  OP shifts from  $1349$  to  $1337\text{ cm}^{-1}$ . Moreover, it is possible to see a change in the relative intensity of the two peaks, with the bands of the cis conformer becoming more intense than the band related to the trans conformer. Moreover, other peaks related to the  $\text{TFSI}^-$  anion show interaction when NaFSI is added; specifically, we can appreciate the shift of the band related to  $\text{CF}_3$  ( $1051$  to  $1056\text{ cm}^{-1}$ ) and S-N stretching ( $780$  to  $799\text{ cm}^{-1}$ ). The shift in these peaks has already been observed in the literature for Na and Li systems [29,61]. In the FTIR region assigned to the bands of C=O and C-O (Figure 6), it is interesting to observe how the relative intensity of the peaks for the neat polymer is very low, making it difficult to identify the peak positions. However, when Na salt is added, both peaks show an increase in intensity, although no peak shift can be appreciated. A shift was also observed for this material in bands related to the cation groups in the  $[\text{PDADMA}]^+$  region, where a shift in the peak related to the C-N environment is seen, namely the peak of C-N bending (from  $1669$  to  $1663\text{ cm}^{-1}$ ) (Figure S11).

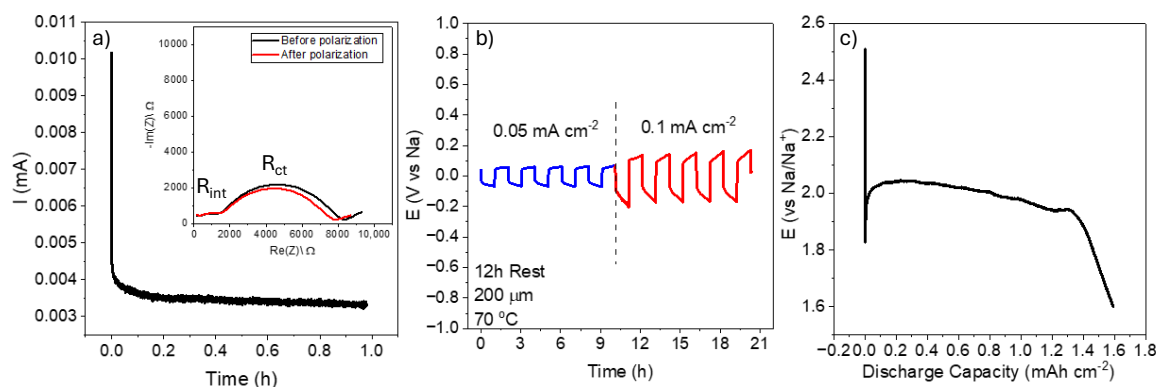


**Figure 6.** (a)  $I$  vs. time of the symmetric Na | BCP-1233-Na | Na cell at 70 °C, polarized with a potential of 10 mV (inset: EIS spectra before and after polarization); (b) galvanostatic cycling of sodium symmetrical cells using BCP-1233-Na at 70 °C; (c) discharge curve with BCP-1233-Na as polymer electrolyte at 50 °C. The surface of the air cathode was wetted with 50  $\mu\text{L}$  of NaTFSI/DGME/ $\text{C}_4\text{mpyrTFSI}$ . Applied current:  $75 \mu\text{A cm}^{-2}$ ; cut-off potential: 1.6 V.

In the spectrum of BCP-2318-Na (pink solid line), we observe the same shift observed in BCP-1233-Na for the PDADMATFSI block, but we can see changes in the peaks related to the PVB block as well. Notably, the peak related to the C-O at  $1264 \text{ cm}^{-1}$  shifts to  $1270 \text{ cm}^{-1}$ , and there is the appearance of a shoulder at higher wavenumbers. The peak related to C=O shows changes as well, with the relative intensity of the peak sensibly decreasing when NaFSI is added to the neat BCP-1218 polymer. Contrary to the observations made for BCP-1233-Na, in this case, the peaks lessen in intensity when Na salt is added to the neat polymer.

Moving on to BCP-2333-Na and BCP-1218-Na (Figure S11), similar behavior as observed for BCP-2318-Na can be appreciated, as can the shifting and variation in relative intensity of the same peaks for both PDADMATFSI and PVB blocks.

Looking at the results obtained from FTIR analysis, we can find a trend across all four samples, where BCP-1233 behaves differently from all other polymers. When NaFSI is added to BCP-1233, only the PDADMATFSI coordination with the Na ion is apparent. On the other hand, when NaFSI is added to BCP-1218, BCP-2333, and BCP-2318 in the same NaFSI:PDADMATFSI (2:1) mol ratio, the change in the FTIR peaks of the PVB block suggests a coordination of Na ions with this block as well (Figure S11). It is, however, interesting to note that the  $^{23}\text{Na}$  NMR suggests the population of sodium ions coordinated with the PVB is similar for all systems apart from the BCP-2318, which is a little contradictory to the NMR. This difference could be associated with different time scales for vibrational versus NMR spectroscopies.

## 2.2. Electrochemical Properties and Applicability of Triblock Polymer Electrolytes in a Na-O<sub>2</sub> Battery

From the physicochemical characterization studies above, it was shown that the polymer electrolyte BCP-1233-Na, featuring extended chains of PDADMATFSI and shorter chains of PVB and with a Na:DADMATFSI molar ratio of 2:1, exhibited the highest ionic conductivity at 70 °C among the various compositions explored, prompting the exploration of its electrochemical properties.

The  $\text{Na}^+$  transference number ( $t_{\text{Na}^+}$ ) is a crucial parameter in the development of polymer electrolytes, as an optimal transference number is imperative for ensuring stable charge-discharge performance and prolonged cell cyclability. Employing the Bruce-Vincent method, the  $\text{Na}^+$  transference number for the 1:2 composition was determined. Figure 6a illustrates the current-time curve plot employed for transference number calculation, and the impedance spectrum of Na/1:2 electrolyte/Na before and after this polarization step as an inset in Figure 6a. The obtained transference number at 70 °C was found to be 0.33, comparable to, or higher than, other systems. For instance, sodium (fluorosulfonyl)(n-

nonafluorobutanesulfonyl)imide (Na[(FSO<sub>2</sub>)(n-C<sub>4</sub>F<sub>9</sub>SO<sub>2</sub>)N], NaFNFSI) mixed with PEO (EO:Na<sup>+</sup> = 15) and PDADMATFSI: NaFSI (1:2) exhibited  $t_{\text{Na}^+}$  values of 0.24 at 80 °C and 0.34 at 70 °C, respectively [29,62].

Notably, the EIS spectra before and after polarization show high charge transfer ( $R_{\text{ct}}$ ) and interfacial ( $R_{\text{int}}$ ) resistance, which are represented by the second and third semicircles at mid- and low-frequency ranges, respectively.  $R_{\text{ct}}$  and  $R_{\text{int}}$  are respectively related to the ion diffusion and/or formation of a passivation layer at the surface of the Na metal surface [43].

To further assess cycling stability with reactive Na metal electrodes, Na|Na symmetrical cells were constructed. Figure 6b depicts Na|BCP1233-Na|Na symmetrical cells undergoing galvanostatic cycling at 70 °C for 0.05 and 0.1 mA cm<sup>-2</sup>. The overpotential at 0.05 and 0.1 mA cm<sup>-2</sup> was 100 mV and 200 mV, respectively. However, at a higher current density (0.2 mA cm<sup>-2</sup>), the cells experienced rapid short-circuiting. After 17 cycles at 0.1 mA cm<sup>-2</sup>, the cells underwent a short circuit, as depicted in Figure S12, revealing the presence of prominent dendrites, highlighted by red circles in Figure S13. This phenomenon is likely linked to the heterogeneity of the membrane surface observed through SEM (Figures S14 and S15), leading to poor electric field distribution during cycling and thus promoting specific sites for sodium accumulation and facilitating dendrite formation. As mentioned previously, the cell shows  $R_{\text{ct}}$  and  $R_{\text{int}}$ , which may also be related to poor contact or the formation of an interlayer between the polymer electrolyte and the Na metal, further explaining the rapid decay in the electrochemical performance.

Nevertheless, the cycling performance of the Na metal electrode was sufficient to allow us to study the potential applicability of this block copolymer electrolyte membrane, BCP-1233-Na, in a sodium–oxygen cell.

Figure S16 shows the cell configuration of the Na–O<sub>2</sub> system used. The surface of the air cathode was wetted with 50 µL of NaTFSI/DGME/C<sub>4</sub>mpyrTFSI. The liquid electrolyte chosen to improve the contact between the cathode and the polymer electrolyte was chosen because prior studies indicated that this hybrid electrolyte resulted in good stability against superoxide anion, oxygen, and moisture, and more importantly, the discharge products were more homogeneous in size (≈3.5 µm) and coverage (3.1 cubes mm<sup>-2</sup>) [63]. Figure 6c shows the deep discharge curves with BCP-1233-Na as a polymer electrolyte at 50 °C. The discharge profile presents an initial spike, followed by a plateau at 2.0 V, resembling the typical discharge profile of Na–O<sub>2</sub> [63–65]. The cell shows a discharge capacity of 1.59 mAh cm<sup>-2</sup> with a current density of 75 µA cm<sup>-2</sup>. The discharge capacity observed is higher than that of other quasi-solid-state Na–O<sub>2</sub> systems, demonstrating the potential of the solid polymer electrolyte investigated based on the PVB-PDADMATFSI-PVB block copolymer for application in Na–O<sub>2</sub>. For example, a bilayer electrolyte composed of an ionogel and an ionic liquid (0.5 M NaTFSI in [C<sub>4</sub>mpyr][TFSI], in poly(ethylene glycol) diacrylate (PEGDA) (90:10 wt%)) showed a discharge capacity of 0.19 mAh cm<sup>-2</sup> [66]. Another quasi-solid-state Na–O<sub>2</sub> cell employing NASICON as electrolyte and single-walled carbon nanotubes (SWNTs) and 1-ethyl-3-methylimidazolium ([C<sub>2</sub>C<sub>1</sub>im]) bis (trifluoromethylsulfonyl) imide ([NTf<sub>2</sub>]) showed 1.57 mA cm<sup>-2</sup> discharge capacity with a 1 V cut-off potential at 0.5 mA cm<sup>-2</sup> [67].

### 3. Conclusions

In this work, we have prepared and investigated novel triblock copolymers based on PDADMA TFSI as the ionophilic block and PVB as the more ionophobic structural block. It was revealed that the relative chain length of each block had a significant impact on the  $T_g$  and conductivity of the polymer electrolytes prepared by adding a 2:1 NaFSI:PDADMA to the copolymer. From FTIR and NMR analyses, it was shown that the PVB blocks also coordinated to some extent with the Na<sup>+</sup> ions, in particular when  $M_w$  was higher than that of the PDADMA, as in the BCP-2318-Na material. The highest conductivity was achieved with a higher  $M_w$  of the PDADMATFSI block (BCP-1233-Na), with the greatest mobility suggested by the <sup>23</sup>Na NMR spectra for this system. Finally, the electrochemical behavior

in this latter system was investigated in a Na/Na symmetric cell at 70 °C and at 50 °C for a Na–O<sub>2</sub> cell, indicating the considerable promise and viability of the investigated polymer electrolyte for sodium batteries. This research further opens new avenues for designing novel polymer electrolytes based on block copolymers and reiterates the importance of careful choice of the  $M_w$  of each block. Additional engineering to improve the membrane homogeneity as well as the electrode/solid electrolyte interface for optimizing their potential is under current investigation.

**Supplementary Materials:** The following supporting information can be downloaded at: <https://www.mdpi.com/article/10.3390/batteries10040125/s1>, Experimental Section, Figure S1: H-NMR (300 MHz) di functional CTA X-PAm-DiEst-PAm-X in D<sub>2</sub>O; Figure S2: MALDI-TOF analysis of X-Pam-DiEst-Pam-X (X-AdA-X); Figure S3: H NMR (300 MHz) of MacroCTA in D<sub>2</sub>O; Figure S4 H-NMR of PVB<sub>11.5K</sub>-b-PDADMATFSI<sub>33K</sub>-b-PVB<sub>11.5K</sub>; Figure S5 H-NMR of PVB<sub>11.5K</sub>-b-PDADMATFSI<sub>17.5K</sub>-b-PVB<sub>11.5K</sub>; Figure S6 H-NMR of PVB<sub>22.5K</sub>-b-PDADMATFSI<sub>33K</sub>-b-PVB<sub>22.5K</sub>; Figure S7 H-NMR of PVB<sub>22.5K</sub>-b-PDADMATFSI<sub>17.5K</sub>-b-PVB<sub>22.5K</sub>; Table S1: FTIR absorption band positions and assignment for neat PVB-PDADMAT-PVB BCPs; Figure S8: TEM images of BCP BCP-1233 and BCP-2218; Table S2: Sample name and characteristics of the membrane with 2:1 Na:PDADMATFSI mol ratio for all four compositions of neat polymer; Figure S9: TEM images of BCP BCP-1233-Na and BCP-2218-Na; Figure S10: Ratio between integrals of the two coordination peaks observed in <sup>23</sup>Na NMR; Figure S11: FTIR spectra of neat BCP and BCP-NaFSI mixtures with a 2:1 Na:PDADMA mol ratio; Figure S12: Galvanostatic cycling of sodium symmetrical cells using BCP-1233-Na at 70 °C; Figure S13: Photo of the membrane after galvanostatic cycling in Na | Na cells showing the formation of large dendrites; Figure S14: SEM images of the surface of BCP-1233-Na and BCP-2218-Na, and EDS layered image zoomed on one of the structures found on the surface of BCP-2218-Na; Figure S15: SEM images of the cross-section of BCP-1233(2); Figure S16: Cell configuration of the home modified Swagelok-type Na-O<sub>2</sub> cell used.

**Author Contributions:** P.L.S., material synthesis, sample preparation, physiochemical characterization, electrochemical characterization, and manuscript preparation, A.G. material synthesis, physiochemical characterization, results discussion, and revised manuscript, C.V.-S. material preparation, M.A. electrochemical characterization and results discussion, A.K. electrochemical characterization and results discussion, L.A.O. NMR characterization, results discussion, and revised manuscript, J.F. material synthesis and revised manuscript, D.M. project conception, supervision, results discussion, and revised manuscript, C.P.-G. supervision, results discussion, and revised manuscript, M.F. supervision, project conception, results discussion, and manuscript preparation. All authors have read and agreed to the published version of the manuscript.

**Funding:** This project received funding from the European Union’s Horizon 2020 research and innovation program under the Marie Skłodowska-Curie grant agreement No. 860403. The authors acknowledge the Australian Research Council (ARC) for funding through Discovery Programme DP160101178 and the ARC Industry Transformation Training Centre for Future Energy Technologies (storEnergy) for funding under grant agreement No. IC180100049.

**Data Availability Statement:** The original contributions presented in the study are included in the article/Supplementary Materials, further inquiries can be directed to the corresponding author.

**Conflicts of Interest:** All authors declare that they have no conflicts of interest.

## References

1. Wu, F.; Maier, J.; Yu, Y. Guidelines and Trends for Next-Generation Rechargeable Lithium and Lithium-Ion Batteries. *Chem. Soc. Rev.* **2020**, *49*, 1569–1614. [[CrossRef](#)] [[PubMed](#)]
2. Masias, A.; Marcicki, J.; Paxton, W.A. Opportunities and Challenges of Lithium Ion Batteries in Automotive Applications. *ACS Energy Lett.* **2021**, *6*, 621–630. [[CrossRef](#)]
3. Mauger, A.; Julien, C.M.; Paoletta, A.; Armand, M.; Zaghbi, K. Building Better Batteries in the Solid State: A Review. *Materials* **2019**, *12*, 3892. [[CrossRef](#)]
4. Yang, J.; Zhang, H.; Zhou, Q.; Qu, H.; Dong, T.; Zhang, M.; Tang, B.; Zhang, J.; Cui, G. Safety-Enhanced Polymer Electrolytes for Sodium Batteries: Recent Progress and Perspectives. *ACS Appl. Mater. Interfaces* **2019**, *11*, 17109–17127. [[CrossRef](#)] [[PubMed](#)]
5. Skundin, A.M.; Kulova, T.L.; Yaroslavtsev, A.B. Sodium-Ion Batteries (a Review). *Russ. J. Electrochem.* **2018**, *54*, 113–152. [[CrossRef](#)]

6. Kulova, T.L.; Fateev, V.N.; Seregina, E.A.; Grigoriev, A.S. A Brief Review of Post-Lithium-Ion Batteries. *Int. J. Electrochem. Sci.* **2020**, *15*, 7242–7259. [[CrossRef](#)]
7. Yin, H.; Han, C.; Liu, Q.; Wu, F.; Zhang, F.; Tang, Y.; Yin, H.; Wu, F.Y.; Tang, Y.B.; Han, C.J.; et al. Recent Advances and Perspectives on the Polymer Electrolytes for Sodium/Potassium-Ion Batteries. *Small* **2021**, *17*, 2006627. [[CrossRef](#)] [[PubMed](#)]
8. Gebert, F.; Knott, J.; Gorkin, R.; Chou, S.L.; Dou, S.X. Polymer Electrolytes for Sodium-Ion Batteries. *Energy Storage Mater.* **2021**, *36*, 10–30. [[CrossRef](#)]
9. Delmas, C. Sodium and Sodium-Ion Batteries: 50 Years of Research. *Adv. Energy Mater.* **2018**, *8*, 1703137. [[CrossRef](#)]
10. Zhao, C.; Liu, L.; Qi, X.; Lu, Y.; Wu, F.; Zhao, J.; Yu, Y.; Hu, Y.S.; Chen, L. Solid-State Sodium Batteries. *Adv. Energy Mater.* **2018**, *8*, 1703012. [[CrossRef](#)]
11. Chen, F.; Wang, X.; Armand, M.; Forsyth, M. Cationic Polymer-in-Salt Electrolytes for Fast Metal Ion Conduction and Solid-State Battery Applications. *Nat. Mater.* **2022**, *21*, 1175–1182. [[CrossRef](#)] [[PubMed](#)]
12. Eftekhari, A.; Saito, T. Synthesis and Properties of Polymerized Ionic Liquids. *Eur. Polym. J.* **2017**, *90*, 245–272. [[CrossRef](#)]
13. Forsyth, M.; Porcarelli, L.; Wang, X.; Goujon, N.; Mecerreyes, D. Innovative Electrolytes Based on Ionic Liquids and Polymers for Next-Generation Solid-State Batteries. *Acc. Chem. Res.* **2019**, *52*, 686–694. [[CrossRef](#)] [[PubMed](#)]
14. Li, Z.Y.; Li, Z.; Fu, J.L.; Guo, X. Sodium-Ion Conducting Polymer Electrolytes. *Rare Met.* **2023**, *42*, 1–16. [[CrossRef](#)]
15. An, Y.; Han, X.; Liu, Y.; Azhar, A.; Na, J.; Nanjundan, A.K.; Wang, S.; Yu, J.; Yamauchi, Y. Progress in Solid Polymer Electrolytes for Lithium-Ion Batteries and Beyond. *Small* **2022**, *18*, 2103617. [[CrossRef](#)]
16. Wang, H.; Sheng, L.; Yasin, G.; Wang, L.; Xu, H.; He, X. Reviewing the Current Status and Development of Polymer Electrolytes for Solid-State Lithium Batteries. *Energy Storage Mater.* **2020**, *33*, 188–215. [[CrossRef](#)]
17. Rollo-Walker, G.; Malic, N.; Wang, X.; Chiefari, J.; Forsyth, M.; Lufano, F.; Aricò, A.S.; Baglio, V.; Chiefari@csiro, J.; Au, J.C. Development and Progression of Polymer Electrolytes for Batteries: Influence of Structure and Chemistry. *Polymers* **2021**, *13*, 4127. [[CrossRef](#)]
18. Loo, W.S.; Galluzzo, M.D.; Li, X.; Maslyn, J.A.; Oh, H.J.; Mongcopa, K.I.; Zhu, C.; Wang, A.A.; Wang, X.; Garetz, B.A.; et al. Phase Behavior of Mixtures of Block Copolymers and a Lithium Salt. *J. Phys. Chem. B* **2018**, *122*, 8065–8074. [[CrossRef](#)] [[PubMed](#)]
19. Young, W.S.; Kuan, W.F.; Epps, T.H. Block Copolymer Electrolytes for Rechargeable Lithium Batteries. *J. Polym. Sci. B Polym. Phys.* **2014**, *52*, 1–16. [[CrossRef](#)]
20. Ding, P.; Lin, Z.; Guo, X.; Wu, L.; Wang, Y.; Guo, H.; Li, L.; Yu, H. Polymer Electrolytes and Interfaces in Solid-State Lithium Metal Batteries. *Mater. Today* **2021**, *51*, 449–474. [[CrossRef](#)]
21. Alipoori, S.; Mazinani, S.; Aboutalebi, S.H.; Sharif, F. Review of PVA-Based Gel Polymer Electrolytes in Flexible Solid-State Supercapacitors: Opportunities and Challenges. *J. Energy Storage* **2020**, *27*, 101072. [[CrossRef](#)]
22. Wu, F.; Zhang, K.; Liu, Y.; Gao, H.; Bai, Y.; Wang, X.; Wu, C. Polymer Electrolytes and Interfaces toward Solid-State Batteries: Recent Advances and Prospects. *Energy Storage Mater.* **2020**, *33*, 26–54. [[CrossRef](#)]
23. Arefin, A.M.E.; Khatri, N.R.; Kulkarni, N.; Egan, P.F. Polymer 3D Printing Review: Materials, Process, and Design Strategies for Medical Applications. *Polymers* **2021**, *13*, 1499. [[CrossRef](#)] [[PubMed](#)]
24. Feng, H.; Lu, X.; Wang, W.; Kang, N.G.; Mays, J.W. Block Copolymers: Synthesis, Self-Assembly, and Applications. *Polymers* **2017**, *9*, 494. [[CrossRef](#)]
25. Dau, H.; Jones, G.R.; Tsogtgerel, E.; Nguyen, D.; Keyes, A.; Liu, Y.S.; Rauf, H.; Ordonez, E.; Puchelle, V.; Basbug Alhan, H.; et al. Linear Block Copolymer Synthesis. *Chem. Rev.* **2022**, *122*, 14471–14553. [[CrossRef](#)]
26. Zarrintaj, P.; Ramsey, J.D.; Samadi, A.; Atoufi, Z.; Yazdi, M.K.; Ganjali, M.R.; Amirabad, L.M.; Zangene, E.; Farokhi, M.; Formela, K.; et al. Poloxamer: A Versatile Tri-Block Copolymer for Biomedical Applications. *Acta Biomater.* **2020**, *110*, 37–67. [[CrossRef](#)]
27. Huang, C.; Zhu, Y.; Man, X. Block Copolymer Thin Films. *Phys. Rep.* **2021**, *932*, 1–36. [[CrossRef](#)]
28. Karayianni, M.; Pispas, S. Block Copolymer Solution Self-Assembly: Recent Advances, Emerging Trends, and Applications. *J. Polym. Sci.* **2021**, *59*, 1874–1898. [[CrossRef](#)]
29. Malunavar, S.; Gallastegui, A.; Wang, X.; Makhlooghiyazad, F.; Mecerreyes, D.; Armand, M.; Galceran, M.; Howlett, P.C.; Forsyth, M. Formulation and Characterization of PS-Poly(Ionic Liquid) Triblock Electrolytes for Sodium Batteries. *ACS Appl. Polym. Mater.* **2022**, *4*, 8977–8986. [[CrossRef](#)]
30. Liu, C.; Hong, C.Y.; Pan, C.Y. Polymerization Techniques in Polymerization-Induced Self-Assembly (PISA). *Polym. Chem.* **2020**, *11*, 3673–3689. [[CrossRef](#)]
31. Cornel, E.J.; Jiang, J.; Chen, S.; Du, J. Principles and Characteristics of Polymerization-Induced Self-Assembly with Various Polymerization Techniques. *CCS Chem.* **2021**, *3*, 2104–2125. [[CrossRef](#)]
32. Yagci, Y.; Tasdelen, M.A. Mechanistic Transformations Involving Living and Controlled/Living Polymerization Methods. *Prog. Polym. Sci.* **2006**, *31*, 1133–1170. [[CrossRef](#)]
33. Moad, G.; Rizzardo, E.; Thang, S.H. RAFT Polymerization and Some of Its Applications. *Chem. Asian J.* **2013**, *8*, 1634–1644. [[CrossRef](#)] [[PubMed](#)]
34. Shah, N.J.; Dadashi-Silab, S.; Galluzzo, M.D.; Chakraborty, S.; Loo, W.S.; Matyjaszewski, K.; Balsara, N.P. Effect of Added Salt on Disordered Poly(Ethylene Oxide)-Block-Poly(Methyl Methacrylate) Copolymer Electrolytes. *Macromolecules* **2021**, *54*, 1414–1424. [[CrossRef](#)]
35. Kulkarni, A.A.; Doerk, G.S.; Saavedra, H.M.; Mullen, T.J.; Zhang, P.; Wu, S.-L.; Javier, A.E. Block Copolymers as (Single-Ion Conducting) Lithium Battery Electrolytes. *Nanotechnology* **2021**, *33*, 062002. [[CrossRef](#)]

36. Coote, J.P.; Adotey, S.K.J.; Sangoro, J.R.; Stein, G.E. Interfacial Effects in Conductivity Measurements of Block Copolymer Electrolytes. *ACS Polym. Au* **2023**, *3*, 331–343. [[CrossRef](#)]
37. Lingua, G.; Grysan, P.; Vlasov, P.S.; Verge, P.; Shaplov, A.S.; Gerbaldi, C. Unique Carbonate-Based Single Ion Conducting Block Copolymers Enabling High-Voltage, All-Solid-State Lithium Metal Batteries. *Macromolecules* **2021**, *54*, 6911–6924. [[CrossRef](#)] [[PubMed](#)]
38. Wang, X.; Chen, F.; Girard, G.M.A.; Zhu, H.; MacFarlane, D.R.; Mecerreyes, D.; Armand, M.; Howlett, P.C.; Forsyth, M. Poly(Ionic Liquid)s-in-Salt Electrolytes with Co-Coordination-Assisted Lithium-Ion Transport for Safe Batteries. *Joule* **2019**, *3*, 2687–2702. [[CrossRef](#)]
39. Demarteau, J.; Fernandez De Anastro, A.; Shaplov, A.S.; Mecerreyes, D. Poly(Diallyldimethylammonium) Based Poly(Ionic Liquid) Di- and Triblock Copolymers by PISA as Matrices for Ionogel Membranes. *Polym. Chem.* **2020**, *11*, 1481–1488. [[CrossRef](#)]
40. Wang, X.; Girard, G.M.A.; Zhu, H.; Yunis, R.; Macfarlane, D.R.; Mecerreyes, D.; Bhattacharyya, A.J.; Howlett, P.C.; Forsyth, M. Poly(Ionic Liquid)s/Electrospun Nanofiber Composite Polymer Electrolytes for High Energy Density and Safe Li Metal Batteries. *ACS Appl. Energy Mater.* **2019**, *2*, 6237–6245. [[CrossRef](#)]
41. Bhandary, R.; Schönhoff, M. Polymer Effect on Lithium Ion Dynamics in Gel Polymer Electrolytes: Cationic versus Acrylate Polymer. *Electrochim. Acta* **2015**, *174*, 753–761. [[CrossRef](#)]
42. Brinkkötter, M.; Lozinskaya, E.I.; Ponkratov, D.O.; Vlasov, P.S.; Rosenwinkel, M.P.; Malyshkina, I.A.; Vygodskii, Y.; Shaplov, A.S.; Schönhoff, M. Influence of Anion Structure on Ion Dynamics in Polymer Gel Electrolytes Composed of Poly(Ionic Liquid), Ionic Liquid and Li Salt. *Electrochim. Acta* **2017**, *237*, 237–247. [[CrossRef](#)]
43. Makhlooghiyazad, F.; Mejía, L.M.G.; Rollo-Walker, G.; Kourati, D.; Galceran, M.; Chen, F.; Deschamps, M.; Howlett, P.; O'Dell, L.A.; Forsyth, M. Understanding Polymerized Ionic Liquids as Solid Polymer Electrolytes for Sodium Batteries. *J. Am. Chem. Soc.* **2024**, *146*, 1992–2004. [[CrossRef](#)] [[PubMed](#)]
44. Young, W.S.; Epps, T.H. Ionic Conductivities of Block Copolymer Electrolytes with Various Conducting Pathways: Sample Preparation and Processing Considerations. *Macromolecules* **2012**, *45*, 4689–4697. [[CrossRef](#)]
45. Cao, X.H.; Li, J.H.; Yang, M.J.; Yang, J.L.; Wang, R.Y.; Zhang, X.H.; Xu, J.T. Simultaneous Improvement of Ionic Conductivity and Mechanical Strength in Block Copolymer Electrolytes with Double Conductive Nanophases. *Macromol. Rapid Commun.* **2020**, *41*, 1900622. [[CrossRef](#)] [[PubMed](#)]
46. Forsyth, M.; Hilder, M.; Zhang, Y.; Chen, F.; Carre, L.; Rakov, D.A.; Armand, M.; Macfarlane, D.R.; Pozo-Gonzalo, C.; Howlett, P.C. Tuning Sodium Interfacial Chemistry with Mixed-Anion Ionic Liquid Electrolytes. *ACS Appl. Mater. Interfaces* **2019**, *11*, 43093–43106. [[CrossRef](#)] [[PubMed](#)]
47. Hilder, M.; Gras, M.; Pope, C.R.; Kar, M.; Macfarlane, D.R.; Forsyth, M.; O'Dell, L.A. Effect of Mixed Anions on the Physicochemical Properties of a Sodium Containing Alkoxyammonium Ionic Liquid Electrolyte. *Phys. Chem. Chem. Phys.* **2017**, *19*, 17461–17468. [[CrossRef](#)] [[PubMed](#)]
48. Kerner, M.; Plylahan, N.; Scheers, J.; Johansson, P. Ionic Liquid Based Lithium Battery Electrolytes: Fundamental Benefits of Utilising Both TFSI and FSI Anions? *Phys. Chem. Chem. Phys.* **2015**, *17*, 19569–19581. [[CrossRef](#)]
49. Kim, S.J.; Yoon, S.G.; Kim, I.Y.; Kim, S.I. Swelling Characterization of the Semiinterpenetrating Polymer Network Hydrogels Composed of Chitosan and Poly(Diallyldimethylammonium Chloride). *J. Appl. Polym. Sci.* **2004**, *91*, 2876–2880. [[CrossRef](#)]
50. Li, S.; Zhang, Z.; Yang, K.; Yang, L. Polymeric Ionic Liquid-Poly(Ethylene Glycol) Composite Polymer Electrolytes for High-Temperature Lithium-Ion Batteries. *ChemElectroChem* **2018**, *5*, 328–334. [[CrossRef](#)]
51. Coussirat, V.; Amarilla, F.; Peruzzo, P.J.; Cortizo, M.S. Dioctyl Fumarate-Co-Vinyl Benzoate Copolymers Preparation and Their Performance as Flow Improvers in Waxy Crude Oils. *J. Pet. Sci. Eng.* **2019**, *182*, 106290. [[CrossRef](#)]
52. Jebrane, M.; Sèbe, G. A New Process for the Esterification of Wood by Reaction with Vinyl Esters. *Carbohydr. Polym.* **2008**, *72*, 657–663. [[CrossRef](#)]
53. Yunis, R.; Girard, G.M.A.; Wang, X.; Zhu, H.; Bhattacharyya, A.J.; Howlett, P.; MacFarlane, D.R.; Forsyth, M. The Anion Effect in Ternary Electrolyte Systems Using Poly(Diallyldimethylammonium) and Phosphonium-Based Ionic Liquid with High Lithium Salt Concentration. *Solid State Ion.* **2018**, *327*, 83–92. [[CrossRef](#)]
54. Nguyen, H.D.; Kim, G.T.; Shi, J.; Paillard, E.; Judeinstein, P.; Lyonard, S.; Bresser, D.; Iojoiu, C. Nanostructured Multi-Block Copolymer Single-Ion Conductors for Safer High-Performance Lithium Batteries. *Energy Environ. Sci.* **2018**, *11*, 3298–3309. [[CrossRef](#)]
55. Chintapalli, M.; Le, T.N.P.; Venkatesan, N.R.; Mackay, N.G.; Rojas, A.A.; Thelen, J.L.; Chen, X.C.; Devaux, D.; Balsara, N.P. Structure and Ionic Conductivity of Polystyrene-Block-Poly(Ethylene Oxide) Electrolytes in the High Salt Concentration Limit. *Macromolecules* **2016**, *49*, 1770–1780. [[CrossRef](#)]
56. Mohan, V.M.; Raja, V.; Sharma, A.K.; Rao, V.V.R.N. Ionic Conductivity and Discharge Characteristics of Solid-State Battery Based on Novel Polymer Electrolyte (PEO + NaBiF<sub>4</sub>). *Mater. Chem. Phys.* **2005**, *94*, 177–181. [[CrossRef](#)]
57. Yoon, H.; Zhu, H.; Hervault, A.; Armand, M.; MacFarlane, D.R.; Forsyth, M. Physicochemical Properties of N-Propyl-N-Methylpyrrolidinium Bis(Fluorosulfonyl)Imide for Sodium Metal Battery Applications. *Phys. Chem. Chem. Phys.* **2014**, *16*, 12350–12355. [[CrossRef](#)]
58. Herstedt, M.; Smirnov, M.; Johansson, P.; Chami, M.; Grondin, J.; Servant, L.; Lassègues, J.C. Spectroscopic Characterization of the Conformational States of the Bis(Trifluoromethanesulfonyl)Imide Anion (TFSI<sup>-</sup>). *J. Raman Spectrosc.* **2005**, *36*, 762–770. [[CrossRef](#)]

59. Umebayashi, Y.; Mitsugi, T.; Fukuda, S.; Fujimori, T.; Fujii, K.; Kanzaki, R.; Takeuchi, M.; Ishiguro, S.I. Lithium Ion Solvation in Room-Temperature Ionic Liquids Involving Bis(Trifluoromethanesulfonyl) Imide Anion Studied by Raman Spectroscopy and DFT Calculations. *J. Phys. Chem. B* **2007**, *111*, 13028–13032. [[CrossRef](#)]
60. Sanchez-Cupido, L.; Pringle, J.M.; Siriwardana, A.I.; Hilder, M.; Forsyth, M.; Pozo-Gonzalo, C. Correlating Electrochemical Behavior and Speciation in Neodymium Ionic Liquid Electrolyte Mixtures in the Presence of Water. *ACS Sustain. Chem. Eng.* **2020**, *8*, 14047–14057. [[CrossRef](#)]
61. Pont, A.L.; Marcilla, R.; De Meazza, I.; Grande, H.; Mecerreyes, D. Pyrrolidinium-Based Polymeric Ionic Liquids as Mechanically and Electrochemically Stable Polymer Electrolytes. *J. Power Sources* **2009**, *188*, 558–563. [[CrossRef](#)]
62. Ma, Q.; Liu, J.; Qi, X.; Rong, X.; Shao, Y.; Feng, W.; Nie, J.; Hu, Y.S.; Li, H.; Huang, X.; et al. A New Na[(FSO<sub>2</sub>)(n-C<sub>4</sub>F<sub>9</sub>SO<sub>2</sub>)N]-Based Polymer Electrolyte for Solid-State Sodium Batteries. *J. Mater. Chem. A Mater.* **2017**, *5*, 7738–7743. [[CrossRef](#)]
63. Ortiz-Vitoriano, N.; Monterrubio, I.; Garcia-Quintana, L.; López Del Amo, J.M.; Chen, F.; Rojo, T.; Howlett, P.C.; Forsyth, M.; Pozo-Gonzalo, C. Highly Homogeneous Sodium Superoxide Growth in Na-O<sub>2</sub> Batteries Enabled by a Hybrid Electrolyte. *ACS Energy Lett.* **2020**, *5*, 903–909. [[CrossRef](#)]
64. Ortiz Vitoriano, N.; Ruiz de Larramendi, I.; Sacci, R.L.; Lozano, I.; Bridges, C.A.; Arcelus, O.; Enterría, M.; Carrasco, J.; Rojo, T.; Veith, G.M. Goldilocks and the Three Glymes: How Na<sup>+</sup> Solvation Controls Na–O<sub>2</sub> Battery Cycling. *Energy Storage Mater.* **2020**, *29*, 235–245. [[CrossRef](#)]
65. Wang, J.; Ni, Y.; Liu, J.; Lu, Y.; Zhang, K.; Niu, Z.; Chen, J. Room-Temperature Flexible Quasi-Solid-State Rechargeable Na-O<sub>2</sub> Batteries. *ACS Cent. Sci.* **2020**, *6*, 1955–1963. [[CrossRef](#)]
66. Ha, T.A.; Fdz De Anastro, A.; Ortiz-Vitoriano, N.; Fang, J.; MacFarlane, D.R.; Forsyth, M.; Mecerreyes, D.; Howlett, P.C.; Pozo-Gonzalo, C. High Coulombic Efficiency Na-O<sub>2</sub> Batteries Enabled by a Bilayer Ionogel/Ionic Liquid. *J. Phys. Chem. Lett.* **2019**, *10*, 7050–7055. [[CrossRef](#)]
67. Chang, S.; Hou, M.; Xu, B.; Liang, F.; Qiu, X.; Yao, Y.; Qu, T.; Ma, W.; Yang, B.; Dai, Y.; et al. High-Performance Quasi-Solid-State Na-Air Battery via Gel Cathode by Confining Moisture. *Adv. Funct. Mater.* **2021**, *31*, 2011151. [[CrossRef](#)]

**Disclaimer/Publisher’s Note:** The statements, opinions and data contained in all publications are solely those of the individual author(s) and contributor(s) and not of MDPI and/or the editor(s). MDPI and/or the editor(s) disclaim responsibility for any injury to people or property resulting from any ideas, methods, instructions or products referred to in the content.